Tradeoff Analysis of Factors Affecting Longitudinal Carrier Landing Performance for Small UAV Based on Backstepping Controller

Zheng Fengying (郑峰婴)[1*], *Gong Huajun* (龚华军)[2], *Zhen Ziyang* (甄子洋)[2]

1. College of Astronautics, Nanjing University of Aeronautics and Astronautics, Nanjing 210016, P. R. China;
2. College of Automation Engineering, Nanjing University of Aeronautics and Astronautics, Nanjing 210016, P. R. China

(Received 20 May 2014; revised 16 December 2014; accepted 12 January 2015)

Abstract: Tradeoff analysis of the factors, including external environment and unmanned aerial vehicle (UAV) aerodynamic attributes, which affect longitudinal carrier landing performance, is important for small UAV. First, small UAV longitudinal carrier landing system is established, as well as the nonlinear dynamics and kinematics model, and then the longitudinal flight control system using backstepping technology with minimum information about the aerodynamic is designed. To assess the landing performance, a variety of influencing factors are considered, resulting in the constraints of aerodynamic attributes of carrier UAV. The simulation results show that the severe sea condition has the greatest influence on landing dispersion, while air wake is the primary factor on impact velocity. Among the longitudinal aerodynamic parameters, the lift curve slope is the most important factor affecting the landing performance, and increasing lift curve slope can improve the landing performance significantly. A better system performance will be achieved when the lift curve slope is larger than 2 per radian.

Key words: unmanned aerial vehicle (UAV); backstepping control; aerodynamic attributes; landing performance

CLC number: V249.1 **Document code**: A **Article ID**: 1005-1120(2015)01-0097-13

0 Introduction

Unmanned systems are becoming increasingly important for military application. Recent naval wars have demonstrated that unmanned air vehicles (UAVs) play a vital role in the future of the Navy[1]. Since researches on carrier-based UAV are just in an initial period[2-3], published literatures in this area are relatively limited. Miniaturization is the trend of the carrier-based UAV[3]. However, the small UAV is more vulnerable to the influences of its aerodynamic attributes and external disturbances due to its small size and lightweight, which should be considered in design.

In terms of affecting factors, three main sources are considered for external disturbances. First of all, due to the waves, the motion of the ship is a six degrees of freedom motion, causing the desired touchdown point to be a three-dimensional zone. Secondly, the carrier aircraft will be disturbed not only by conventional atmospheric turbulence, but by carrier running stern formed cocktail airflow and deck pitch motion[4]. Additionally, navigation error is another factor that affects the landing accuracy. For aircraft aerodynamic attributes, various literatures suggest that longitudinal aerodynamic characteristics are the important affecting factors on piloted land-based aircraft landing performance. As for automated carrier landing control, most researches focus mainly on classical or robust linear control methods[5-6]. However, when the aircraft passes through a highly nonlinear dynamic region or other complicated control objectives are set, it is difficult to obtain practical controllers based on line-

* **Corresponding author**: Zheng Fengying, Assistant Researcher, E-mail: zhfy@nuaa.edu.cn.

How to cite this article: Zheng Fengying, Gong Huajun, Zhen Ziyang. Tradeoff analysis of factors affecting longitudinal carrier landing performance for small UAV based on backstepping controller[J]. Trans. Nanjing U. Aero. Astro., 2015, 32(1): 97-109.

http://dx.doi.org/10.16356/j.1005-1120.2015.01.097

ar design techniques. The UAV shipboard recovery task is substantially a nonlinear problem.

Nonlinear control with the ability in solving such tough problems should be the next logical step for automated carrier landing systems. However, few researches have been done in the area of applying nonlinear controllers to UAV carrier landing system. One of previous endeavors in nonlinear aircraft carrier landing systems was made by Denison[7]. He evaluated an automated carrier landing system utilizing a nonlinear dynamic inversion control scheme to achieve acceptable performance and robustness for a wide range of sea-state and atmospheric conditions. Additionally, Steinberg et al.[8-9] expanded his investigation into the application of several different nonlinear control schemes to automated carrier landing system, including dynamic inversion, fuzzy logic, and neural networks. These researches show that nonlinear control is a good option for future carrier landing system.

Feedback linearization has been used to handle the nonlinear equations of motion, generating controllers suitable for the entire flight envelope[10-12]. An approach to design flight control laws with feedback linearization is to utilize the two time-scale separation assumptions that separate the fast dynamics from the slow. But the inherent drawback is that the calculated gain of the inner controller needs to be large enough to guarantee closed-loop stability[13]. It may excite unmodeled dynamics or saturate the control inputs, thus leading to a robustness problem.

The variable structure control (VSC) with sliding mode is another widely used nonlinear control method, whose drawback is that the sliding mode algorithm needs continuous switching logic which may fall into the chattering phenomenon and drive the high frequency modes of unmodeled dynamics[14-15].

Backstepping control without chattering problem offers a more flexible way to deal with nonlinearities than feedback linearization. It is an effective technique based on Lyapunov theory to design control algorithms for the system with a cascade structure. Stabilizing nonlinearities can be kept in the closed loop system while destabilizing ones cancelled.

The backstepping method for constructing stable nonlinear controllers can improve the flight control system. Numerous applications of the backstepping control techniques for flight control can be found in literatures. Sharma et al. presented a neural adaptive backstepping controller that provided excellent command tracking and robustness against the aerodynamic uncertainties[16]. Jung and Tsiotras considered the problem of path following control for a small fixed wing UAV using backstepping control in their work[17]. Hemanshu et al. obtained a novel backstepping-based velocity control method for unmanned helicopters[18].

Factors affecting the performance of longitudinal carrier landing performance for small UAV are analyzed in this paper. In order to guarantee that the effects of aircraft attributes are not shadowed by gain variances in the controller, a backstepping control law with the minimum information of the aerodynamic model is proposed. The roll of the controller is to enable the system to track the UAV velocity and flight path angle, thus realizing flight trajectory control by using the elevator deflection and the engine thrust as actuators.

Simulations are carried out based on a realistic UAV model. The detailed data of the nonlinear longitudinal model of small carried-UAV, such as the aircraft geometry and the aerodynamic coefficients can be obtained from Ref. [3].

1 Longitudinal Automatic Carrier Landing System for Small UAV

The small carrier UAV longitudinal landing simulation system used to assess landing performance is constructed as shown in Fig. 1. The ship motion model and navigation error model are provided by the Naval Air Systems Command (NAVAIR)[3,19], and an airwake model is given by MIL-F-8785C military specification[20]. The flight

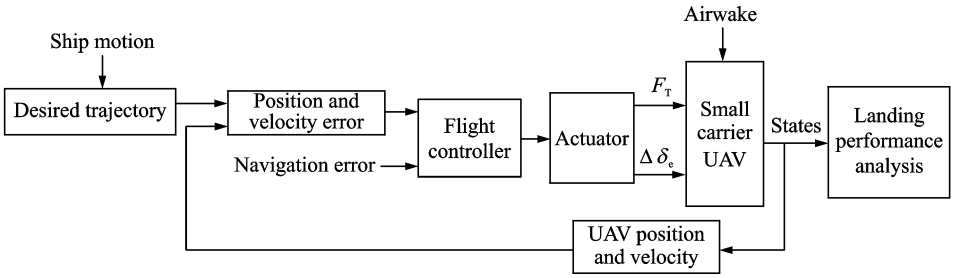

Fig. 1 Structural allocation of small carrier UAV longitudinal landing system

controller uses backstepping technique, and a ten-millisecond time step (0.01 s) is selected to match the models.

Main longitudinal landing performance index of carrier aircraft includes landing impact velocity, mean and standard deviation of the longitudinal position error, the longitudinal deviation range, boarding rate, etc (Table 1). In addition, American Military Standard MIL-A-8863 indicates that the allowable minimum value of carrier-based aircraft impact velocity is 0.914 m/s[21], however, the constraint of impact velocity is different in various aircraft-carrier systems. Although the impact velocity of carrier landing system is calculated in the simulation, it is not a symbol of successful landing.

Table 1 Longitudinal performance index

Performance index	Target performance	Allowable performance
Horizontal mean deviation/m	4.88	7.32
Horizontal standard deviation/m	12.2	18.2
Horizontal deviation range/m	−6.1—6.1	−12.2—12.2
Vertical deviation range/m	−0.76—1.52	−1.52—3.05
Boarding rate/%	75	65

Terminal error equations are used to evaluate the landing performance. The terminal error equations of vertical deviation, horizontal deviation, and impact velocity are as follows[22]

$$\Delta h_{TD} = h - (h_s - L_{TD} \cdot \theta_s + Y_{TD} \cdot \phi_s)$$

$$\Delta x_{TD} \doteq \frac{1}{\gamma}\Delta h_{TD}$$

$$\Delta V_{TD} = \dot{h}_s - L_{TD} \cdot \dot{\theta}_s + V_R \cdot \theta_s - V_R \cdot \sin\psi_d \phi_s - \dot{h} \tag{1}$$

where Δh_{TD} and Δx_{TD} are the vertical and horizontal landing errors of aircraft, respectively. ΔV_{TD} is the impact velocity of landing point, h the virtual flight height. h_s, θ_s and ϕ_s are the ship up-down, pitch and roll motion, respectively. L_{TD} and Y_{TD} are the horizontal and lateral distances from the ship′s centre of motion to the desire touchdown point (DTP). γ is the flight path angle, ψ_d the deck angle to ship centerline, V_R the ground speed of the aircraft, and

$$\begin{aligned} V_R &= V - V_{w/d} \\ V_{w/d} &= V_{wind} + V_{ship} \end{aligned} \tag{2}$$

where V is the true airspeed, V_{wind} the natural wind speed, $V_{w/d}$ the wind-over-deck (WOD) speed, and V_{ship} the ship′s forward speed.

The terminal error characteristics in time domain $\Delta h_{TD}(t)$, $\Delta x_{TD}(t)$ and $\Delta V_{TD}(t)$ can be obtained from simulation firstly. Then, the mean deviation and root mean square (RMS) of terminal error can be got from Eq. (3).

$$\begin{cases} \bar{x} = \sum_{i=1}^{n} x_i / n \\ \sigma(x) = \sqrt{\dfrac{\sum_{i=1}^{n} (x_i - \bar{x})^2}{n}} \end{cases} \tag{3}$$

where x_i is the ith sample of stochastic process and n the sample size.

2 Longitudinal Control System for Small UAV

2.1 Small UAV nonlinear longitudinal model

Considering the nonlinear longitudinal model of a carrier-based UAV[3], let $[h, x, V, \gamma, \theta, q] \in \mathbf{R}^6$ be the state vector, where h is the flight height, x the horizontal distance to touchdown

point, θ the pitch angle, q the pitch angular velocity, and $[F_T, \delta_e] \in \mathbf{R}^2$ the control input vectors, here F_T is the engine thrust and δ_e the elevator angle. The longitudinal equation of the UAV can be written as

$$\begin{aligned}
\dot{h} &= V\sin\gamma \\
\dot{x} &= V\cos\gamma \\
\dot{V} &= (-D + F_T\cos\alpha - mg\sin\gamma)/m \\
\dot{\gamma} &= \frac{1}{mV}(L + F_T\sin\alpha - mg\cos\gamma) \\
\dot{\theta} &= q \\
\dot{q} &= \frac{M(\delta_e)}{I_y}
\end{aligned} \tag{4}$$

where m and I_y are the mass and the inertia. L, D and $M(\delta_e)$ the aerodynamics lift, drag and pitching moment, respectively. Fig. 2 gives a detailed definition of the forces, moments, and velocities. Note that $\theta = \alpha + \gamma$, where α is the angle of attack.

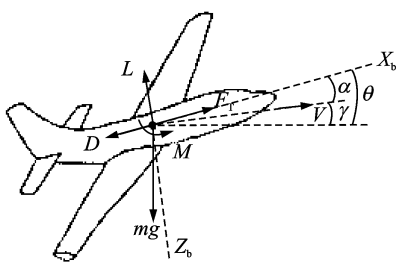

Fig. 2 Definition of forces, moments and angles

As usual in aerodynamic modeling, the aerodynamic forces and moments are computed through their non-dimensional coefficients as follows

$$L = \frac{1}{2}\rho V^2 S C_L,\ D = \frac{1}{2}\rho V^2 S C_D,\ M = \frac{1}{2}\rho V^2 S\bar{c} C_m \tag{5}$$

where ρ is the air density, S the reference wing surface, $\bar{c}$ the mean chord, and C_L, C_D, C_m the lift, drag and pitching moment coefficients, respectively. Moreover, we consider the following models for the lift, drag and moment coefficients.

$$\begin{aligned}
C_L &= C_{L0} + C_{L\alpha}\alpha + C_{L\delta_e}\delta_e \\
C_D &= C_{D0} + A_{polar}C_L + A_2 C_L^2 \\
C_m &= C_{m0} + C_{m\alpha}\alpha + C_{mq}q + C_{m\delta_e}\delta_e
\end{aligned} \tag{6}$$

where C_{L0}, C_{D0}, $C_{L\alpha}$, $C_{L\delta_e}$, A_{polar}, A_2, C_{m0}, $C_{m\alpha}$, C_{mq} and $C_{m\delta_e}$ are the aircraft aerodynamic coefficients.

Assumption 1 The lift coefficient C_L is only a function of α, that is $C_{L\delta_e} = 0$, and the reference axis X_b is parallel to the aircraft zero-lift line, $C_{L0} = 0$. The assumption is satisfied by conventional airplanes in the non-stalled regime. Then, the property $x \cdot C_L(x) \geqslant 0$ is satisfied for all $x \in \mathbf{R}$.

2.2 Longitudinal backstepping controller design

In this case, the outputs of interest are velocity perturbation, height and horizontal deviation. According to Eq. (4), V and γ, as two values, are selected to ensure precise trajectory tracking. The controller is required to simultaneously maintain the desired velocity and desired flight path angle as precisely as possible.

To simplify the controller design, we consider first velocity dynamic and then the flight path angle dynamic. Thus, two different controllers are designed as: the velocity is controlled using thrust (F_T), and the flight path angle is controlled with the elevator angle (δ_e).

2.2.1 Control of velocity

From Eq. (4), the velocity dynamic reads

$$\dot{V} = [-\frac{1}{2}\rho V^2 S(C_{D0} + A_{polar}C_L + A_2 C_L^2) + F_T\cos\alpha - mg\sin\gamma]/m \tag{7}$$

where the engine thrust F_T is the control input, while α and γ are considered measurable.

Denote V_r as the reference velocity and define the error $z_v = V - V_r$, $f_v = -\frac{\rho S}{2m}V^2 C_D$.

Thus, the evolution of error becomes

$$\dot{z}_v = \dot{V} - \dot{V}_r = f_v + F_T\frac{\cos\alpha}{m} - g\sin\gamma - \dot{V}_r \tag{8}$$

Proposition 1 Consider Eq. (8), then the stable feedback given by Eqs. (9—11) guarantees global boundedness of z_v.

$$F_T^0 = -\frac{m}{\cos\alpha}(-g\sin\gamma - \dot{V}_r + f_v + k_v z_v + r_v\lambda_v) \tag{9}$$

where k_v is a positive definite gain, and $\lambda_v = \int_0^t \bar{z}_v \mathrm{d}t$ the integral term used to achieve zero steady-state error, $\bar{z}_v$ is to be defined. F_T^0 is forced to generate the magnitude, rate and bandwidth limited con-

trol signal F_T through command filter [23-24].

The effect of implementing the limited control law instead of the desired one can again be estimated with

$$\dot{\zeta}_v = -k_v\zeta_v + \frac{\cos\alpha}{m}(F_T - F_T^0) \tag{10}$$

The compensated velocity tracking error is

$$\bar{z}_v = z_v - \zeta_v \tag{11}$$

Proof Define the Lyapunov function as

$$W_v = \frac{1}{2}(\bar{z}_v^2 + r_v\lambda_v^2) \tag{12}$$

Take the derivative of W_v

$$\dot{W}_v = \bar{z}_v\dot{\bar{z}}_v + r_v\lambda_v\dot{\lambda}_v \tag{13}$$

Substitute Eqs. (8—11) into Eq. (13)

$$\dot{W}_v = \bar{z}_v\dot{\bar{z}}_v + r_v\lambda_v\dot{\lambda}_v = \bar{z}_v(\dot{z}_v - \dot{\zeta}_v) + r_v\lambda_v\bar{z}_v =$$
$$\bar{z}_v\left[f_v + F_T\frac{\cos\alpha}{m} - g\sin\gamma - \dot{V}_r + k_v\zeta_v - \frac{\cos\alpha}{m}(F_T - F_T^0)\right] + r_v\lambda_v\bar{z}_v =$$
$$\bar{z}_v\left(f_v - g\sin\gamma - \dot{V}_r + k_v\zeta_v + \frac{\cos\alpha}{m}F_T^0\right) +$$
$$r_v\lambda_v\bar{z}_v = \bar{z}_v(f_v - g\sin\gamma - \dot{V}_r + k_v\zeta_v +$$
$$g\sin\gamma + \dot{V}_r - f_v - k_v z_v - c_v\lambda_v) +$$
$$r_v\lambda_v\bar{z}_v = -k\bar{z}_v^2 \tag{14}$$

Thus, since W_v is the positive definition and radically unbounded and $\dot{W}_v \leqslant 0$ then, by LaSalle-Yoshizawa theorem we conclude global boundedness of $\bar{z}_v$ and convergence of $\bar{z}_v$ to zero.

2.2.2 Control of flight path angle

From controlling purpose, the flight path angle dynamics can be rewritten as

$$\dot{\gamma} = \frac{1}{mV}\left(\frac{1}{2}\rho V^2 SC_L + F_T\sin\alpha - mg\cos\gamma\right) \tag{15}$$

$$\dot{\theta} = q \tag{16}$$

$$\dot{q} = \frac{\rho V^2 S\bar{c}}{2\cdot I_y}(C_{m0} + C_{m\alpha}\alpha + C_{mq}q + C_{m\delta_e}\delta_e) \tag{17}$$

where V and F_T are obtained in the previous step design of Subsection 2.2.1.

Assumption 2 The following usual assumptions are made: (1) Since $\gamma \approx \gamma_{ref}$, it is assumed that $\cos\gamma = \cos\gamma_{ref}$, which is proposed in Ref. [25]. (2) γ_{ref} is assumed to be held constant when carrier-based UAV landing. $\dot{\gamma}_{ref}$ is assumed to be zero.

The aircraft engines cannot produce negative thrust. Thus, it is satisfied that $F_T \geqslant 0$.

Under Assumption 2, Eq. (15) becomes

$$\dot{\gamma} = f(\alpha) = f(\theta - \gamma) \tag{18}$$

and the scalar function f is defined as

$$f(\alpha) = \frac{1}{mV}\left(\frac{1}{2}\rho V^2 SC_L(\alpha) + F_T\sin\alpha - mg\cos\gamma_{ref}\right) \tag{19}$$

The control objective is to make the equilibrium $(\gamma,\theta,q) = (\gamma_{ref},\theta_{ref},0)$ asymptotically stable, where γ_{ref} is given and θ_{ref} is computed from equation $\theta_{ref} = \gamma_{ref} + \alpha_0$. α_0 is the trim angle of attack supposed to be known.

In order to design the controller we shift the equilibrium to zero defining the following set of error coordinates

$$x_1 = \gamma - \gamma_{ref},\ x_2 = \theta - \gamma_{ref} - \alpha_0,\ x_3 = q \tag{20}$$

The dynamic equation in the new set of coordinates read

$$\dot{x}_1 = \sigma(x_2 - x_1) \tag{21}$$

$$\dot{x}_2 = x_3 \tag{22}$$

$$\dot{x}_3 = \beta_1[C_{m0} + C_{m\alpha}(x_2 - x_1) + C_{mq}x_3 + C_{m\delta_e}\delta_e] \tag{23}$$

where $\beta_1 = \frac{\rho V^2 S\bar{c}}{2\cdot I_y}$, $\sigma(x) = f(x + \alpha_0)$.

Note that according to Assumption 1, the scalar function $\sigma(x)$ satisfies $x\cdot\sigma(x) \geqslant 0$.

Now the control objective is to stabilize the origin of Eqs. (21—23) (globally) asymptotically, thereby, we stabilize each step of the cascade explicitly using backstepping approach with the minimum information of the aerodynamic model.

Step 1 Eq. (21) is fixed using x_2 as a virtual control. Define the Lyapunov function

$$W_1 = \frac{1}{2}x_1^2 \tag{24}$$

The derivative reads $\dot{W}_1 = x_1\cdot\sigma(x_2 - x_1)$, and then we select the control $x_{2,d} = -k_1x_1$, if $x_2 = x_{2,d}$, then $\dot{W}_1 = x_1\cdot\sigma[-(k_1+1)x_1]$. Hence $\dot{W}_1$ is negative definition for $k_1 > -1$.

Step 2 Define the error variable

$$z_2 = x_2 - x_{2,d} \tag{25}$$

$$\dot{z}_2 = \dot{x}_2 - \dot{x}_{2,d} = x_3 + k_1\dot{x}_1 \tag{26}$$

Let $\xi = x_2 - x_1$, then

$$\dot{\xi} = \dot{x}_2 - \dot{x}_1 = x_3 - \sigma(\xi) \tag{27}$$

The Lyapunov function for Eqs. (25—26) is

$$W_2 = c_1W_1 + \frac{1}{2}z_2^2 + M(\xi) \tag{28}$$

where $c_1 > 0$, $M(\xi)$ is the positive definite function[26] used to avoid cancellations of the terms associated to $\sigma(\xi)$ which would introduce extra terms in the controller. $M(\xi)$ is to be defined further.

By selecting the virtual control as

$$x_{3,\mathrm{d}} = -k_2 z_2 \tag{29}$$

Here, $k_2 > 0$, and define $M'(\xi) = c_2\sigma(\xi)$, $c_2 > 0$. If $x_3 = x_{3,\mathrm{d}}$, then calculate $\dot{W}_2$, we get

$$\begin{aligned}\dot{W}_2 &= c_1\dot{W}_1 + z_2\dot{z}_2 + \dot{M}(\xi) = \\ &c_1 x_1\sigma(\xi) + z_2(x_3 + k_1\sigma(\xi)) + M'(\xi)\dot{\xi} = \\ &c_1 x_1\sigma(\xi) + z_2(-k_2 z_2 + k_1\sigma(\xi)) + M'(\xi)\dot{\xi} = \\ &c_1 x_1\sigma(\xi) - k_2 z_2^2 + k_1\sigma(\xi)z_2 + c_2\sigma(\xi)(-k_2 z_2 - \\ &\sigma(\xi)) = (c_1 x_1 + k_1 z_2 - c_2 k_2 z_2)\sigma(\xi) - \\ &k_2 z_2^2 + c_2\sigma^2(\xi)\end{aligned} \tag{30}$$

Let $c_1 = -(1 + k_1)(k_1 - c_2 k_2)$, and $k_1 < c_2 k_2$, Eq. (30) becomes

$$\begin{aligned}\dot{W}_2 &= (c_1 x_1 + (k_1 - c_2 k_2)z_2)\sigma(\xi) - k_2 z_2^2 - \\ &c_2\sigma^2(\xi) = (-(1 + k_1)x_1 + x_2)(k_1 - \\ &c_2 k_2)\sigma(\xi) - k_2 z_2^2 - c_2\sigma^2(\xi) = (k_1 - c_2 k_2)\xi \cdot \\ &\sigma(\xi) - k_2 z_2^2 - c_2\sigma^2(\xi)\end{aligned} \tag{31}$$

where the first term is negative defined by Assumption 1.

Step 3 To extend the backstepping design for generating the elevator deflection laws. In order to analyze the affecting factor of aircraft attributes, the control law is designed without cancellation of terms coming from $\sigma(\xi)$ in the previous step design.

Consider Eq. (23), and let $g_q = \beta_1 C_{\mathrm{m}_{\delta_e}}$, $f_q = \beta_1[C_{\mathrm{m}0} + C_{\mathrm{m}\alpha}(x_2 - x_1) + C_{\mathrm{m}q}x_3]$. Then Eq. (23) becomes $\dot{x}_3 = f_q + g_q \cdot \delta_e$.

Define the error as $z_3 = x_3 - x_{3,\mathrm{d}}$, then

$$\begin{aligned}\dot{z}_3 &= \dot{x}_3 - \dot{x}_{3,\mathrm{d}} = f_q + g_q \cdot \delta_e + k_2\dot{z}_2 = \\ &f_q + g_q \cdot \delta_e + k_2(z_3 - k_2 z_2 + k_1\sigma(\xi))\end{aligned} \tag{32}$$

The compound Lyapunov function for Step 3 is

$$W_3 = c_3 W_2 + \frac{1}{2}z_3^2 + r\lambda_3^2 \tag{33}$$

where $c_3 > 0$, $\lambda_3 = \int_0^t z_3\,\mathrm{d}t$.

The Lyapunov function derivative becomes

$$\begin{aligned}\dot{W}_3 &= c_3\dot{W}_2 + z_3\dot{z}_3 + r\lambda_3 z_3 = \\ &c_3((k_1 - c_2 k_2)\xi \cdot \sigma(\xi) - k_2 z_2^2 - c_2\sigma^2(\xi) + \\ &z_3(z_2 + c_2\sigma(\xi))) + z_3(f_q + g_q \cdot \delta_e + \\ &k_2(z_3 - k_2 z_2 + k_1\sigma(\xi))) + r\lambda_3 z_3\end{aligned} \tag{34}$$

In Eq. (34), there is a cross-term $z_3\sigma(\xi)$ whose sign is undefined. If it is cancelled, the function $\sigma(\xi)$ will appear and the benefit of the controller shown in the previous backstepping step will be lost. Instead, the terms $\sigma^2(\xi)$, z_3^2 and $z_3\sigma(\xi)$ are grouped and the squares are completed as follows

$$\begin{aligned}&-c_3 c_2\sigma^2(\xi) + (c_2 c_3 + k_1 k_2)z_3\sigma(\xi) = \\ &-[c_3 c_2\sigma^2(\xi) - (c_2 c_3 + k_1 k_2)z_3\sigma(\xi)] - \\ &(\sqrt{c_3 c_2}\,\sigma(\xi) - \frac{c_2 c_3 + k_1 k_2}{2\sqrt{c_3 c_2}}z_3)^2 + \frac{(c_2 c_3 + k_1 k_2)^2}{4 c_3 c_2}z_3^2\end{aligned}$$

Complete the squares also in the cross-terms $z_2 z_3$, we have

$$\begin{aligned}&-c_3 k_2 z_2^2 + c_3 z_2 z_3 - k_2^2 z_2 z_3 = -c_3 k_2 z_2^2 + (c_3 - \\ &k_2^2)z_2 z_3 = -\left[\sqrt{c_3 k_2}\,z_2 - \frac{(c_3 - k_2^2)}{2\sqrt{c_3 k_2}}z_3\right]^2 + \\ &\frac{(c_3 - k_2^2)^2}{4 c_3 k_2}z_3^2\end{aligned}$$

Thus, Eq. (34) can be rewritten as

$$\begin{aligned}\dot{W}_3 &= c_3\dot{W}_2 + z_3\dot{z}_3 + r\lambda_3 z_3 = c_3[(k_1 - c_2 k_2)\xi \cdot \\ &\sigma(\xi) - k_2 z_2^2 - c_2\sigma^2(\xi) + z_3(z_2 + c_2\sigma(\xi))] + \\ &z_3[f_q + g_q \cdot \delta_e + k_2(z_3 - k_2 z_2 + k_1\sigma(\xi))] + \\ &r\lambda_3 z_3 = c_3[(k_1 - c_2 k_2)\xi \cdot \sigma(\xi)] + z_3(f_q + \\ &g_q \cdot \delta_e) + k_2 z_3^2 - \left(\sqrt{c_3 c_2}\,\sigma(\xi) - \right. \\ &\left.\frac{c_2 c_3 + k_1 k_2}{2\sqrt{c_3 c_2}}z_2\right)^2 + \frac{(c_2 c_3 + k_1 k_2)^2}{4 c_3 c_2}z_3^2 - \\ &\left[\sqrt{c_3 k_2}\,z_2 - \frac{(c_3 - k_2^2)}{2\sqrt{c_3 k_2}}z_3\right]^2 + \frac{(c_3 - k_2^2)^2}{4 c_3 k_2}z_3^2 + \\ &k_2 z_3^2 + r\lambda_3 z_3 = c_3[(k_1 - c_2 k_2)\xi \cdot \sigma(\xi)] - \\ &\left[\sqrt{c_3 c_2}\,\sigma(\xi) - \frac{c_2 c_3 + k_1 k_2}{2\sqrt{c_3 c_2}}z_2\right]^2 + z_3[(f_q + \\ &g_q \cdot \delta_e) + \frac{(c_2 c_3 + k_1 k_2)^2}{4 c_3 c_2}z_3 + \frac{(c_3 - k_2^2)^2}{4 c_3 k_2}z_3 + \\ &k_2 z_3] - \left(\sqrt{c_3 k_2}\,z_2 - \frac{c_3 - k_2^2}{2\sqrt{c_3 k_2}}z_3\right)^2 + r\lambda_3 z_3\end{aligned} \tag{35}$$

This derivative is negative definition by choosing the following control with integral term to improve robustness.

$$\delta_e = -\frac{1}{g_q}(k_3 z_3 + f_q + r\lambda_3) \tag{36}$$

with $k_3 > \dfrac{(c_2 c_3 + k_1 k_2)^2}{4 c_3 c_2} + \dfrac{(c_3 - k_2^2)^2}{4 c_3 k_2} + k_2$

We formally summarize the result obtained in the section in the following proposition.

Proposition 2 To consider the system under Assumptions 1 and 2. Then, the state feedback is expressed by

$$\delta_e = -\frac{1}{g_q}[k_3(x_3 - x_{3,d}) + f_q] + r\lambda_3 = -\frac{1}{g_q}\{k_3[x_3 - k_2(x_2 + k_1 x_1)] + f_q\} + r\lambda_3 \tag{37}$$

With c_2, c_3, k_1, k_2, k_3 positive and satisfying

$$k_1 < c_2 k_2,\ k_3 > \frac{(c_2 c_3 + k_1 k_2)^2}{4c_3 c_2} + \frac{(c_3 - k_2^2)^2}{4c_3 k_2} + k_2$$

The global boundedness of (γ, θ, q) is guaranteed.

Proof Note that the proposed Lyapunov function Eq. (33) is positive, together with Eq. (37). Let $\dot{W}_3 \leqslant 0$, and then by LaSalle-Yoshizawa theorem, we conclude global boundedness of (γ, θ, q). It is straightforward to see that the equilibrium manifold $(\gamma, \theta, q) = (\gamma_{ref}, \theta_{ref}, 0)$ is globally asymptotically stable.

2.2.3 Longitudinal control system simulation

Considering carrier-based UAV flight along the glide path, in the process of landing, the trajectory is tracked by regulating flight path angle. Select $\gamma_{ref} = -3.5°$. UAV velocity is commanded to be held constant, and thus reference $V_a = 21$ m/s is selected. Arresting net will absorb aircraft kinetic energy and shorten the slide distance.

Simulation initial conditions are selected as $h_0 = 300$ m/s, $\gamma_0 = 10°$, $V_0 = 30$ m/s. For more realistic simulation, saturations in the control signals are also considered. The following limits are introduced in the thrust and elevator angle $F_T \in [5\text{ N}, 100\text{ N}]$, $\delta_e \in [-25°, 25°]$. Backstepping controller parameters are designed as follows: $k_v = 5.2$, $r_v = 1$, $r_3 = 1$, $k_1 = 0.6$, $k_2 = 3.5$, $k_3 = 10.8$.

Fig. 3 shows the response of the flight control system while inputting unit step longitudinal deviation signal. Fig. 4 indicates the response when inputting the sinusoidal signal with unit ramp signal superimposed amplitude of 1 m, and frequency of 0.5 rad/s.

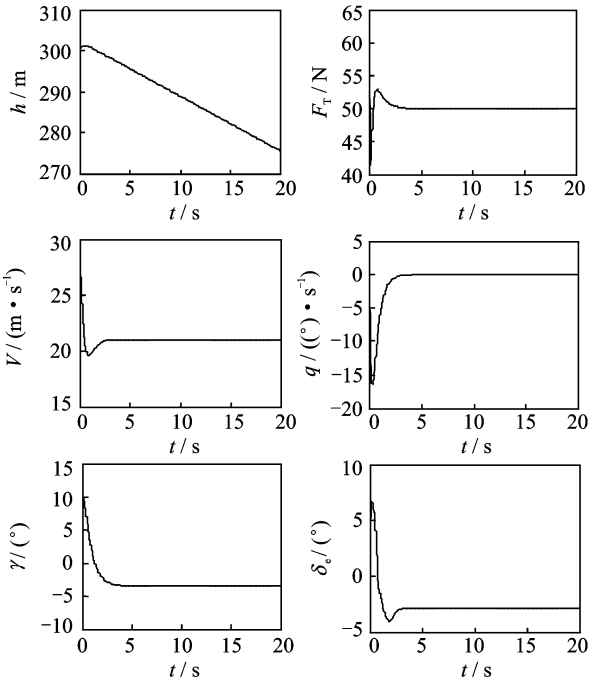

Fig. 3 Flight control system response to unit step command

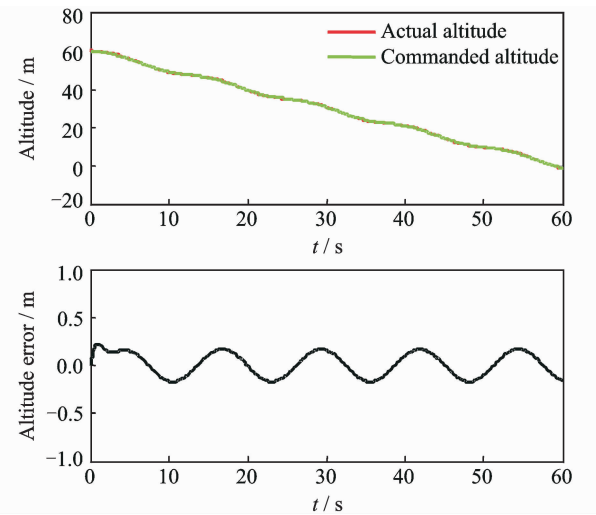

Fig. 4 Flight control system response to the given command

In Figs. 3, 4, the flight control system designed in this paper can track command quickly and accurately. Tracking unit step signal, steady-state error is zero, and control surfaces restore fast. Tracking slope superimposed sinusoidal signal, steady state error does not exceed 0.5 m. Therefore, the designed backstepping controller can be a general control method for small UAV flight control system.

3 Analysis of Performance with Disturbance Sources and Longitudinal Attribute Changes

3.1 Disturbance sources

3.1.1 Ship dynamics

The dynamics and dimensions of the Enterprise Nuclear Aircraft Carrier (CVN 65), are used throughout the research. The distances from the ship's center of motion to desired touchdown point (DTP) are 68 m aft, 19.5 m up, and 3 m lift. Carrier geometry is shown in Fig. 5.

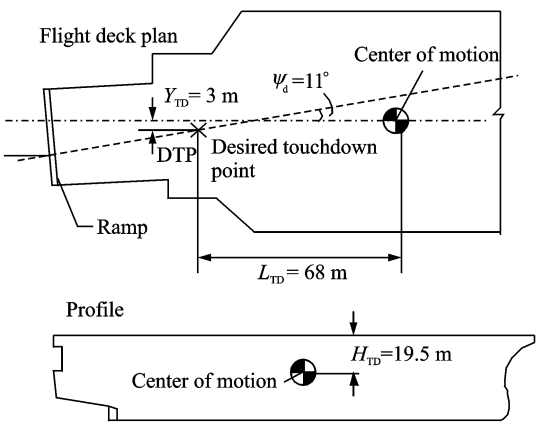

Fig. 5 CVN 65 carrier geometry

The provided ship dynamics model generates six degrees-of-freedom time histories of ship motion for a sea-state selected by the user. Note that all ship displacements are related to the ship center of motion. Since the DTP is displaced a longitudinal distance from the center of motion, the DTP's translational displacements are dependent upon both the translational and angular displacements of the ship. These angles have to be converted to distances X and Z, which are useful in the landing task. Eq. (38) given below is the exact longitudinal relationships.

$$X_{DTP} = 19.5\sin\theta_s + 68\cos\theta_s \cdot \cos\psi_s - 68 - 3\sin\psi_s + x_s$$
$$Z_{DTP} = -68\sin\theta_s + 19.5\cos\theta_s \cdot \cos\phi_s - 19.5 - 10\sin\phi_s + h_s \quad (38)$$

where θ_s, ϕ_s, ψ_s are the pitch, roll and yaw angles of ship, respectively; and x_s, h_s the linear translation of the ship about its center of motion fore or aft, up or down. For the purposes of this research, sea-states 3, 4, and 5 are modeled. Table 2 provides such RMS amplitudes.

Table 2 RMS amplitudes for modeled sea-states

Sea-state	θ_s	ϕ_s	ψ_s	x_s	h_s
3	0.76	0.21	0.12	0.84	2.11
4	1.22	0.33	0.30	1.4	3.81
5	1.83	0.49	0.29	2.1	5.06

The total influence on the vertical displacement of DTP due to ship motion for all three modeled sea-states is presented in Fig. 6.

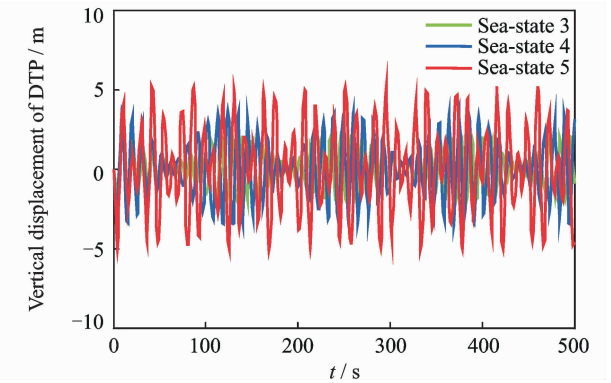

Fig. 6 Vertical displacement of DTP due to ship motion

3.1.2 Airwake model

The MIL-F-8785C military specification gives specific airwake model for carrier landing. The longitudinal (horizontal and vertical) components are composed of four parts: the free atmosphere turbulence component, the wake stead component (cocktail), the wake periodic component, and the wake random component. The detailed calculation process can refer to Ref. [4].

Taking sea-state 3 as an example, UAV speed is set to be $V = 21$ m/s, wind of deck $V_{w/d} = 15$ m/s, initial distance $D_0 = 1\,800$ m, glide slope angle $\gamma_0 = 3.5°$. The total horizontal component u_g and vertical component w_g of airwake are shown in Fig. 7.

3.1.3 Navigation error

Joint precision automated landing system (JPALS) serves as the guidance system on first generation shipboard UAV. JPALS operates using differential global position system (GPS) data blended with inertial navigation on both airplane and carrier. The proximity of the ship and airplane during approach and landing ensures that both GPS receivers experience the same atmospheric disturbance, thus leading to tight error

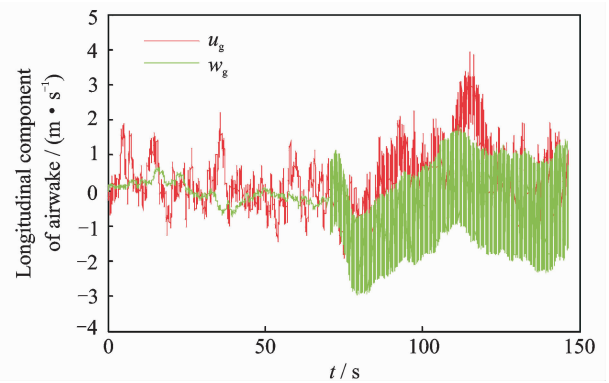

Fig. 7 Result of longitudinal component of airwake simulation

bounds. NAVAIR provides one and a half hours of JPALS flight test data sampled at 50 Hz with both the measured and true positions. Fig. 8 demonstrates navigation error simulation.

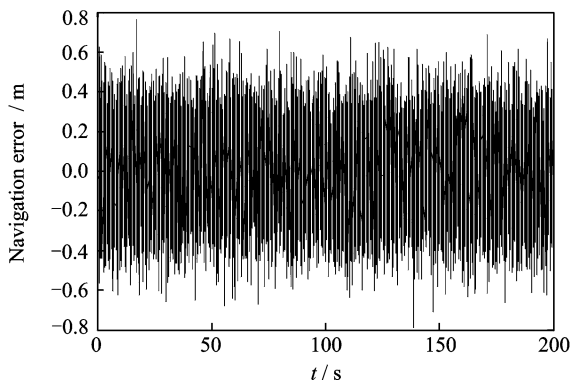

Fig. 8 Navigation error simulation

3.2 Analysis of performance with disturbance sources

To understand the effects of disturbance sources on landing performance, one thousand simulations are conducted with each disturbance source individually, and other simulations are executed with all three disturbance sources. Table 3 shows the simulation results, where "Nav" denotes navigation error added. However, these boarding rates account only for landing position, not for the possibility of extreme touchdown altitudes at which adjustment will be unsuccessful. Moreover, many unpredictable factors are not considered in the simulations. Thus, we narrow landing deviation of allowable range when assessing performance. If the deviation exceeds ±10 m, the landing will be assumed as unsuccessful.

In Table 3, each disturbance source will affect longitudinal landing performance. Navigation error has negligible influence. Landing mean deviation and standard deviation are very small on the case of navigation error only. However, ship motion and airwake have greater influence on landing performance.

From the data, the ship motion is the dominant disturbance source of landing error. The landing performance of only sea-state 4 is worse than sea-state 3 added air wake and navigation error. Sea-state 5 is the most demanding case because of the magnitude of the required flight path changes. The deck moves as much as 10.4 m vertical in 10 s, challenging the system's ability to track a command. Airwake is the main affecting factor on impact velocity. And, no matter which

Table 3 Combination effects of disturbance sources

Case	Condition	Horizontal mean/m	Horizontal std. dev/m	Horizontal deviation/m	Impact velocity/(m • s^{-1})	Boarding rate/%
1	Nav	−0.101 4	0.247 9	−1.071 9—0.669 5	1.446 4—1.595 3	100
2	Airwake(15 *)	−0.346 9	0.854 3	−3.484 13—1.827 0	1.272 6—1.774 5	100
3	Airwake(15), nav	−0.352 4	0.887 4	−3.590 2—2.637 5	1.196 3—1.763 0	100
4	Airwake(20), nav	−0.624 0	0.863 0	−3.770 2—2.210 9	1.244 7—1.758 4	100
5	Sea-state 3	0.196 8	2.555 9	−4.360 0—6.366 4	1.142 2—1.530 4	100
6	Sea-state 3, Airwake(15), nav	0.420 5	2.744 1	−6.018 3—7.517 2	0.747 4—1.906 8	100
7	Sea-state 3, Airwake(20), nav	−0.592 8	2.910 7	−7.340 0—7.969 7	0.748 6—2.273 7	100
8	Sea-state 4	0.728 5	5.094 5	−7.402 0—14.178 7	1.183 6—1.859 1	93
9	Sea-state 4, Airwake(15), nav	0.769 5	5.351 8	−9.537 1—17.727 6	0.502 4—2.509 4	92
10	Sea-state 4, Airwake(20), nav	1.018 2	5.230 4	−10.270—17.903 9	0.515 8—2.842 6	92
11	Sea-state 5	3.363 1	8.706 0	−11.876 4—31.291 9	1.164 3—1.877 2	84
12	Sea-state 5, Airwake(15), nav	3.479 6	8.016 3	−12.839—36.187 6	0.422 9—2.928 4	82
13	Sea-state 5, Airwake(20), nav	3.546 9	8.970 9	−14.315 5—34.814 4	0.223 8—3.172 5	81

* Airwake (15) denotes the value of airwake when WOD = 15 m/s

sea-state selected, once airwake is added, the minimum impact velocity value of one thousand simulations would be less than 0.914 m/s.

Additionally, simulations show that the mean and standard deviation can meet the requirements on all conditions, and landing deviation range can also meet the requirement at sea-state 3. However, landing deviation ranges exceed the target, and have a lower success rate at sea-states 4 and 5.

3.3 Analysis of performance with longitudinal attribute changes

The impact of the longitudinal aerodynamic derivatives C_{L_α}, C_{m_α} and C_{D_α} on small UAV's carrier landing performance is addressed, where, C_{D_α} is the drag coefficient, $C_{D_\alpha} = \partial C_D / \partial_\alpha$.

It should be mentioned that no attempt is made to optimize backstepping controller performance. The purpose is to ensure that the effects of airframe attributes are not shadowed by gain variances in controllers.

3.3.1 Influence of lift curve slope and longitudinal stability

The combined influence of lift curve slope C_{L_α} and longitudinal stability C_{m_α} is evaluated by a combined total of three hundred thousand simulation runs. Lift curve slope C_{L_α} is varied from six-tenths per radian to six per radian in increments of six-tenths per radian. C_{L_α} varies with wing sweep angle and aspect ratio, with lower values of aspect ratio and aft wing sweeps resulting in lower values of lift curve slope C_{L_α}. The longitudinal stability C_{m_α} is varied from negative sixty-five hundredths (stable) to twenty-five hundredths (slightly unstable). C_{m_α} is dependent on the location of the center of gravity relative to the wing's aerodynamic center, where moving the center of gravity aft decreases stability. All other attributes are those for the baseline UAV in the landing configuration. At each combination, one thousand simulated landings are performed for each sea-state, with both airwake and navigation error.

The simulation results show that if the landing position is the only criterion, the autonomous system would have a perfect boarding rate for sea-state 3. Sea-state 3 simulation results yielded no further information are not shown. The boarding rate for Sea-states 4 and 5 are plotted below in Fig. 9, each has lift curve slope increasing up the y-axis and stability decreasing along the x-axis.

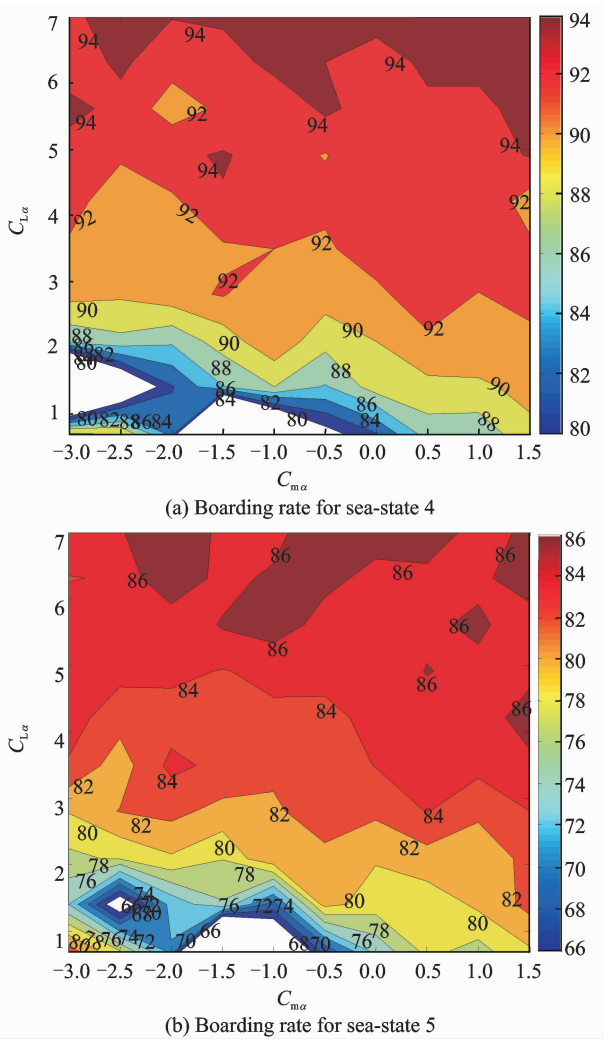

Fig. 9 Sea-state 4 and sea-state 5 boarding rate contour

Fig. 9 (a) illustrates the boarding rate for sea-state 4 ranges from about 80%—94% depending on the aircraft aerodynamic attributes. The lack of smooth contours is attributed to insufficient sample size to fully capture the variability in the ship motion. Fig. 9 (b) shows the same trends more smoothly for sea-state 5 with boarding rates from about 66%—86%. In general, higher lift curve slopes provide higher boarding rates. A C_{L_α} of 2 rad^{-1} or greater is required for target performance. Longitudinal stability has little effect, however, from Fig. 9, we can find that

the landing performance has a better trend with increasing $C_{m\alpha}$.

Boarding rates are strongly related to the landing dispersions. Fig. 10 depicts the landing dispersions for the sea-state 4 and sea-state 5. Recalling the target performance presented in Table 1 is a standard deviation of 12.2 m or less.

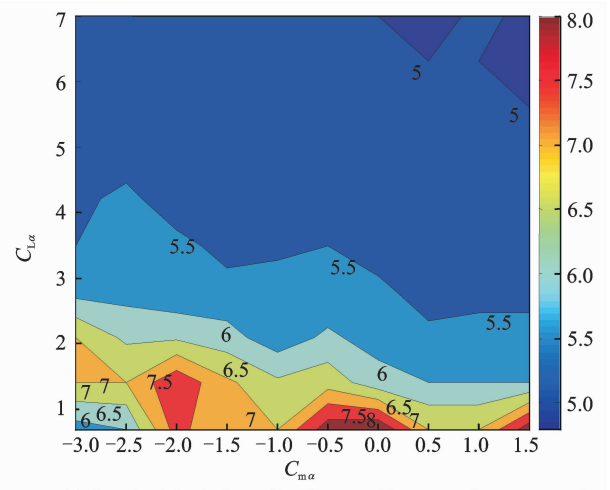

(a) Standard deviation of landing position error for sea-state 4

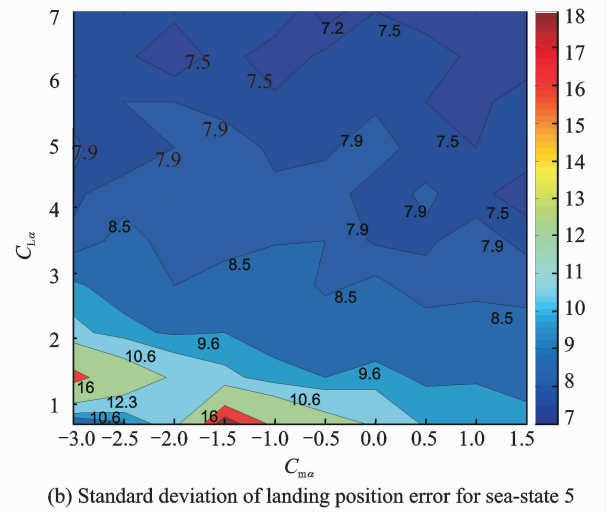

(b) Standard deviation of landing position error for sea-state 5

Fig. 10 Landing position error standard deviation contour for sea-states 4,5

Fig. 10 demonstrates that the minimum acceptable $C_{L\alpha}$ is consistent with the above requirement imposed by boarding rate.

Landing position is not the only concern for carrier-based aircraft. The aircraft's pitch attitude must be tightly controlled to ensure the main gear touchdown first and that the hook will engage properly. Constraining pitch also regulates the angle of attack. Only small variations are permitted to avoid flying approach with a large stall margin, which would drive the approach speed up. Fig. 11 depicts the standard deviation of pitch angle during the simulated approaches at sea-state 5. Greater $C_{L\alpha}$ has smaller pitch attitude, and when $C_{L\alpha}$ is greater than 2 rad^{-1}, pitch attitude is smaller than 4°.

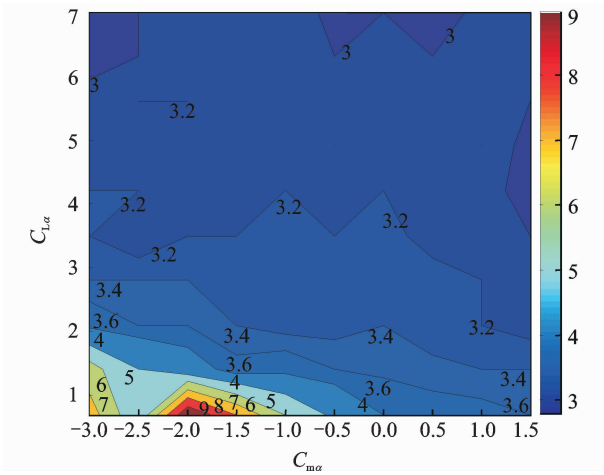

Fig. 11 Standard deviation contour of pitch angle for sea-state 5

3.3.2 Influence of lift curve slope and drag coefficient

The effect of drag coefficient $C_{D\alpha}$ on landing performance is evaluated from 0.008 rad^{-1} to 0.098 rad^{-1} in increments of 0.01 rad^{-1} by varying coefficient A_{polar} . The $C_{L\alpha}$ is varied in exactly the same manner as for the previous section, but $C_{m\alpha}$ is held constant ($C_{m\alpha}=-2.05$ rad^{-1}). Again, one thousand simulations are conducted for each aircraft configuration.

Figs. 12,13 depict the resultant boarding rate and standard deviation of sea-states 4 and 5, respectively. Landing performance is also highly dependent on $C_{L\alpha}$, which improves with $C_{L\alpha}$ increasing. Varying $C_{D\alpha}$ has minimal effects on landing performance.

4 Conclusions

Longitudinal carrier landing performance affecting factors of small UAV based on backstepping controller is studied. The results indicate that:

(1) For realizing carrier performance tradeoff analysis, one designs the backstepping controller for the longitudinal flight dynamics of the small

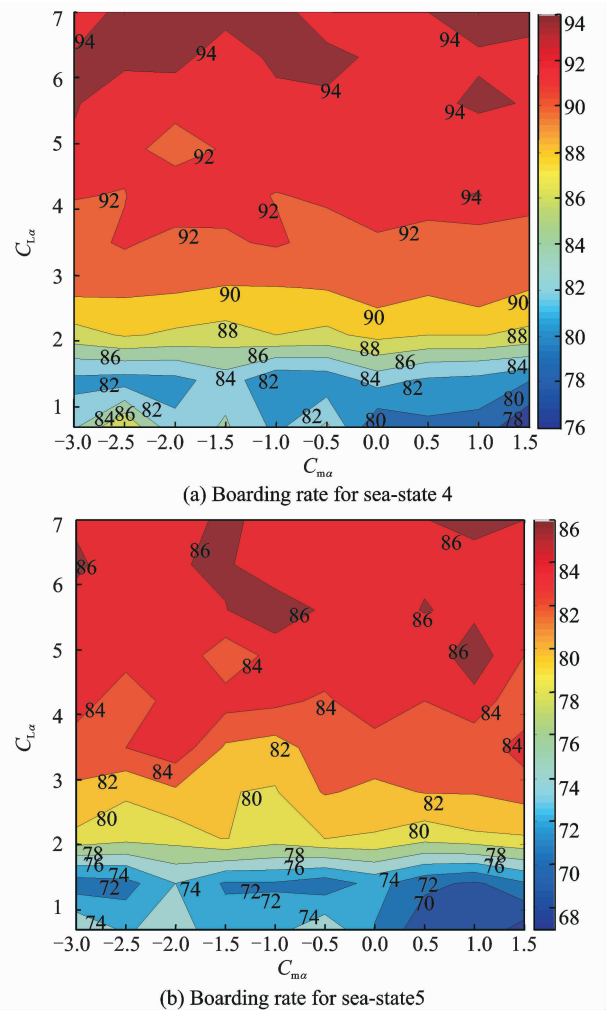

Fig. 12 Boarding rate contour for sea-states 4,5

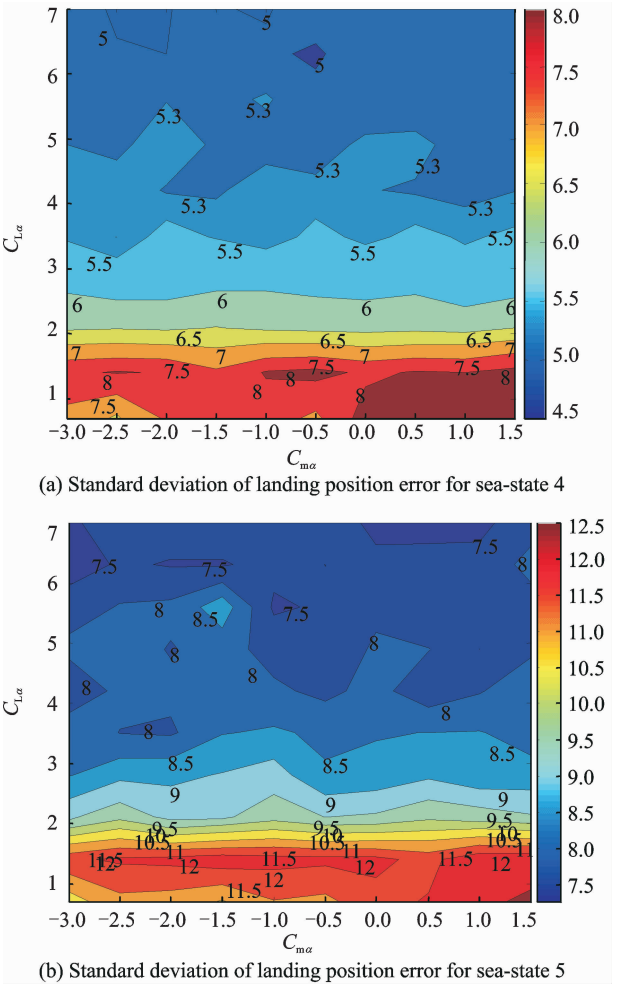

Fig. 13 Landing position error standard deviation contour for sea-states 4,5

UAV to make the aircraft follow commands in velocity and flight path angle to track trajectory. It does not require the entire knowledge of the aerodynamics model and does not need much computational power. In simulations, it is shown that the controller can make the system track the commands, even in the presence of actuator constraints.

(2) Three disturbance sources, including navigation error, airwake and ship motion, are affecting factors on landing performance. Ship motion is the dominant reason of landing position errors, and impact velocity is affected by airwake most.

(3) The lift curve slope $C_{L\alpha}$ is the dominant factor in all aspects of performance for the small UAV carrier-landing task, and increasing $C_{L\alpha}$ improves performance. This is the same result of piloted aircraft. From the simulation, the minimum value of $C_{L\alpha}$ for suitable longitudinal landing performance is 2 rad^{-1}. Carrier-based UAV design must carefully weigh the landing performance benefits of a high lift curve slope, although the minimum lift curve slope requirement constrains the minimum aspect ratio and the maximum wing sweep angle, the two primary geometric attributes of an aircraft.

(4) The longitudinal stability has little influence on landing performance. This is expected because the backstepping controller is continuously updating the control commands. The natural response plays a negligible role in landing performance. Additionally, the drag coefficient also has little effect on landing performance.

Acknowledgements

This work was supported by the National Nature Science Foundation of China (Nos. 61304223, 61403197), the Aeronautical Science Foundation of China (No.

2013ZA52002), and the Research Fund for the Doctoral Program of Higher Education of China (No. 20123218120015).

References:

[1] Zhao T. Development of the shipborne UAVS [J]. Ship Electronic Engineering, 2010, 30(4):21-24. (in Chinese)

[2] Sergey K. Control system design using evolutionary algorithms for autonomous shipboard recovery of unmanned aerial vehicles[D]. Australia: Royal Melbourne Institute of Technology,2006.

[3] Fitzgerald P. Flight control system design for autonomous uav carrier landing[D]. UK: School of Engineering Department of Aerospace Sciences Dynamics, Simulation and Control Group, Cranfield University, 2005.

[4] Yang Y D, Yu J Y. Guidance and control of carrier aircraft landing[M]. Beijing: National Defence Industry Press, 2007. (in Chinese)

[5] Karl E W, Andreas M, Andreas Z. Automatic take off, tracking and landing of a miniature UAV on a moving carrier vehicle[J]. Journal of Intelligent & Robotic Systems, 2011, 61(1/2/3/4):221-238.

[6] Zhu Q, Zhao E J, Zhang W et al. Research of handling characteristics of pilot in carrier landing[C]// Second International Conference on Instrumentation & Measurement, Computer, Communication and Control. Harbin, China: IEEE, 2012.

[7] Denison N A. Automated carrier landing of an unmanned combat aerial vehicle using dynamic inversion [M]. Ensign, USA: Department of The Air Force University, 2007.

[8] Steinberg, Marc L. A fuzzy logic based F/A-18 automatic carrier landing system [C]// Proceedings of the AIAA Guidance, Navigation, and Control Conference. [S. l.]: AIAA, 1992:4392.

[9] Steinberg Marc L, Anthony B. Comparison of neural, fuzzy, evolutionary, and adaptive approaches for carrier landing[C]// Proceedings of the AIAA Guidance, Navigation, and Control Conference. [S. l.]: AIAA, 2001:4085.

[10] Abdulrahman I H, Bajodaha H. Nonlinear generalized dynamic inversion for aircraft maneuvering control[J]. International Journal of Control, 2012, 85(4):437-450.

[11] Jimoh O P, Aarti P, Laurent D. A nonlinear dynamic inversion-based neuro-controller for unmanned combat aerial vehicles during aerial refueling[J]. International Journal of Applied Mathematics and Computer Science,2013,23(1):75-90.

[12] Cai Hongming, Ang Haisong, Zheng Xiangming. Flight control system of MAV based on adaptive dynamic inversion[J]. Journal of Nanjing University of Aeronautics & Astronautics, 2011, 43(2): 137-142. (in Chinese)

[13] Shin D H, Kim Y. Reconfigurable flight control system design using adaptive neural networks[J]. IEEE Transactions on Control Systems Technology, 2004, 12(1): 87-100.

[14] Sun H B, Li S H, Sun C Y. Finite time integral sliding mode control of hypersonic vehicles [J]. Nonlinear Dynamics,2013,73(1/2):229-244.

[15] Du Yanli, Wu Qingxian, Jiang Changsheng. Adaptive predictive control of near-space vehicle using functional link network[J]. Transactions of Nanjing University of Aeronautics & Astronautics, 2010, 27(2): 148-154.

[16] Hemanshu R, Bilal A, Garratt M. Velocity control of a UAV using backstepping control[C]// Proceedings of the 45th IEEE Conference on Decision & Control. San Diego, CA, USA: IEEE, 2006: 5894-5899.

[17] Paw Y C. Attitude control of mini-UAV using backstepping control [J]. Nonlinear Systems Project, 2007:ME8282.

[18] Jung D, Tsiotras P. Bank-to-turn control for a small UAV using backstepping and parameter adaptation [C]//17th IFAC World Congress. Seoul, South Korea:[s. n.],2008:4406-4411.

[19] Rudowsky et al. Review of the carrier approach criteria for carrier-based aircraft phase I: final report [R]. NAWCADPAX/TR-2002/71, Naval Air Systems Command, 2002.

[20] Flying qualities of piloted aircraft. Military Specification MIL-F-8785C[S]. USA: United States Department of Defense.

[21] Airplane strength and rigidity ground loads for navy acquired airplanes MIL-A-8863[S]. USA: United States Department of Defense.

[22] Durand T S, Teper G L. An analysis of terminal flight path control in carrier landing[J]. Systems Technology, TR-137-1, 1964. AD606040.

[23] Jay F, Marios P, Manu S. et al. Command filtered backstepping [J]. IEEE Transactions on Automatic Control,2009,54(6):1391-1395.

[24] Li Hongmei, Pan Jianghuai, He Jiazhou et al. Error transfer and sensitivity analysis of ship-borne radar detecting[J]. Journal of Data Acquisition and Processing, 2012, 27(4): 474-479. (in Chinese)

[25] Kristic M, Kokotovic P V. Lean backstepping design for a jet engine compressor model[C]// IEEE Conference on Control Applications. [S. l.]: IEEE, 1995:1047-1052.

[26] Harkegärd O. Backstepping and control allocation with applications to flight control [D]. Sweden: Linkoping University, 2003.

(Executive editor: Zhang Tong)